Geophysical Research Letters®

RESEARCH LETTER
10.1029/2022GL101320

Megathrust Stress Drop as Trigger of Aftershock Seismicity: Insights From the 2011 Tohoku Earthquake, Japan

A. Dielforder[1], G. M. Bocchini[2], K. Kemna[2], A. Hampel[1], R. M. Harrington[2], and O. Oncken[3]

[1]Institut für Geologie, Leibniz Universität Hannover, Hanover, Germany, [2]Institut für Geologie, Mineralogie und Geophysik, Ruhr-Universität Bochum, Bochum, Germany, [3]GFZ Deutsches GeoForschungsZentrum Potsdam, Potsdam, Germany

Key Points:

- We show using force-balance modeling that a megathrust earthquake stress drop can trigger forearc-wide aftershock seismicity
- Model results explain the Tohoku earthquake aftershock distribution and reveal spatial variability in forearc stress and strength
- Most aftershocks occurred in areas that experienced an increase in deviatoric stress

Supporting Information:

Supporting Information may be found in the online version of this article.

Correspondence to:

A. Dielforder,
dielforder@geowi.uni-hannover.de

Citation:

Dielforder, A., Bocchini, G. M., Kemna, K., Hampel, A., Harrington, R. M., & Oncken, O. (2023). Megathrust stress drop as trigger of aftershock seismicity: Insights from the 2011 Tohoku earthquake, Japan. *Geophysical Research Letters*, *50*, e2022GL101320. https://doi.org/10.1029/2022GL101320

Received 4 NOV 2022
Accepted 21 JAN 2023
Corrected 22 MAR 2023

This article was corrected on 22 MAR 2023. See the end of the full text for details.

Author Contributions:

Conceptualization: A. Dielforder, G. M. Bocchini
Investigation: A. Dielforder, G. M. Bocchini, K. Kemna, A. Hampel, R. M. Harrington, O. Oncken
Methodology: A. Dielforder, G. M. Bocchini, K. Kemna, A. Hampel, R. M. Harrington
Visualization: A. Dielforder, G. M. Bocchini

Abstract Numerous normal-faulting aftershocks in subduction forearcs commonly follow large megathrust earthquakes. Postseismic normal faulting has been explained by stress changes induced by the stress drop along the megathrust. However, details of forearc stress changes and aftershock triggering mechanisms remain poorly understood. Here, we use numerical force-balance models combined with Coulomb failure analysis to show that the megathrust stress drop supports normal faulting, but that forearc-wide aftershock triggering is feasible within a narrow range of megathrust stress drop values and preseismic stress states only. We determine this range for the 2011 Tohoku earthquake (Japan) and show that the associated stress changes explain the aftershock seismicity in unprecedented detail and are consistent with the stress released by forearc seismicity before and after the earthquake.

Plain Language Summary Earthquakes release stresses that build up in the Earth due to the motion of tectonic plates. The stress release can cause additional earthquakes called aftershocks. Several thousand onshore and offshore aftershocks followed the great Tohoku subduction earthquake in March 2011. Whether the stress release of the Tohoku earthquake triggered most of the aftershocks is not well understood, because it is largely unknown how the stress field changed following the earthquake. We therefore use a computer model to estimate the stress release and resulting stress change required to explain the aftershock distribution. We find that 78% of the aftershocks occurred in areas where the Tohoku earthquake caused a subsequent stress increase. Our model results are further consistent with the stress release of smaller earthquakes that occurred in Japan before and after the Tohoku earthquake. Our findings provide new insights into aftershock triggering and help to understand where aftershocks occur after great earthquakes at subduction zones.

1. Introduction

Seismological records indicate that seismicity in forearcs increases after large megathrust earthquakes (Dewey et al., 2007; Hasegawa et al., 2012; Lange et al., 2012). Aftershock seismicity often shows a complex spatial distribution, is highest in the first weeks after the megathrust event, and decays at a power-law like rate ("Omori's law," Parsons, 2002; Toda & Stein, 2022), as exemplified by the 11 March 2011 M_w 9.0 Tohoku earthquake, Japan (Figure 1). The low forearc seismicity in the years before the earthquake focused near the plate interface and volcanic arc (Figures 1a and 1c). Seismicity immediately after the earthquake increased and spread throughout the forearc (Figures 1b and 1d). Seismicity rates were highest in the month following the Tohoku earthquake and decreased rapidly afterward (Figure 1e). The seismicity rate at the end of 2011 decreased by ~95%, but was still higher than before the Tohoku earthquake.

The increase in forearc seismicity indicates that the stress change caused by the megathrust earthquake destabilized the forearc. The exact causes and magnitude of this stress change remain uncertain, although seismological records provide important information on changes in forearc stress. Forearc seismicity after the Tohoku earthquake was dominated by normal faulting (Figure 1d), despite the thrust mechanism of the main shock and prevalence of reverse and strike-slip faulting in the decades preceding it (Hardebeck, 2012; Hasegawa et al., 2012; Yoshida et al., 2012). The normal faulting indicates that the stress state switched from deviatoric compression to deviatoric tension due to the Tohoku earthquake. The stress reversal only occurred in the offshore forearc and coastal regions near Iwaki. Reverse and strike-slip faulting continued inland Japan (Figure 1; Yoshida et al., 2019). Previous studies also inferred similar stress reversals for other megathrust earthquakes, including the 2004 M_w 9.1 Sumatra and 2010 M_w 8.8 Maule earthquakes (Hardebeck, 2012).

Writing – original draft: A. Dielforder, G. M. Bocchini
Writing – review & editing: A. Dielforder, G. M. Bocchini, A. Hampel, R. M. Harrington, O. Oncken

Previous work explained the stress reversal to result from the stress drop of the megathrust earthquake, i.e., the coseismic decrease in megathrust shear stress due to fault weakening processes (Di Toro et al., 2011; Hardebeck, 2012; Hasegawa et al., 2011; Scholz, 1998). The megathrust shear stress loading in the interseismic period causes compression of the forearc (Lamb, 2006; Wang & He, 1999), without which the forearc would experience deviatoric tension due to gravitational stresses resulting from density contrasts and margin topography. If the megathrust shear stress decreases during an earthquake, the loss in compression can cause a reversal from deviatoric compression to deviatoric tension and trigger normal faulting in the forearc (Cubas et al., 2013; Dielforder, 2017; Wang et al., 2019). However, the detailed stress changes caused by the stress drop of megathrust earthquakes like Tohoku remain unresolved. Consequently, it is unknown whether the stress change can explain the broad aftershock seismicity in the forearc.

Aftershock seismicity of megathrust earthquakes has been further investigated by Coulomb failure stress (CFS) models, which test whether the resulting stress changes of an earthquake promote or suppress failure on neighboring faults (Farías et al., 2011; Terakawa et al., 2013; Toda et al., 2011). CFS models for the Tohoku earthquake showed that the stress change promoted some of the aftershocks and likely increased forearc seismicity rates. Aftershock seismicity not promoted by the stress change was interpreted to have been triggered either by

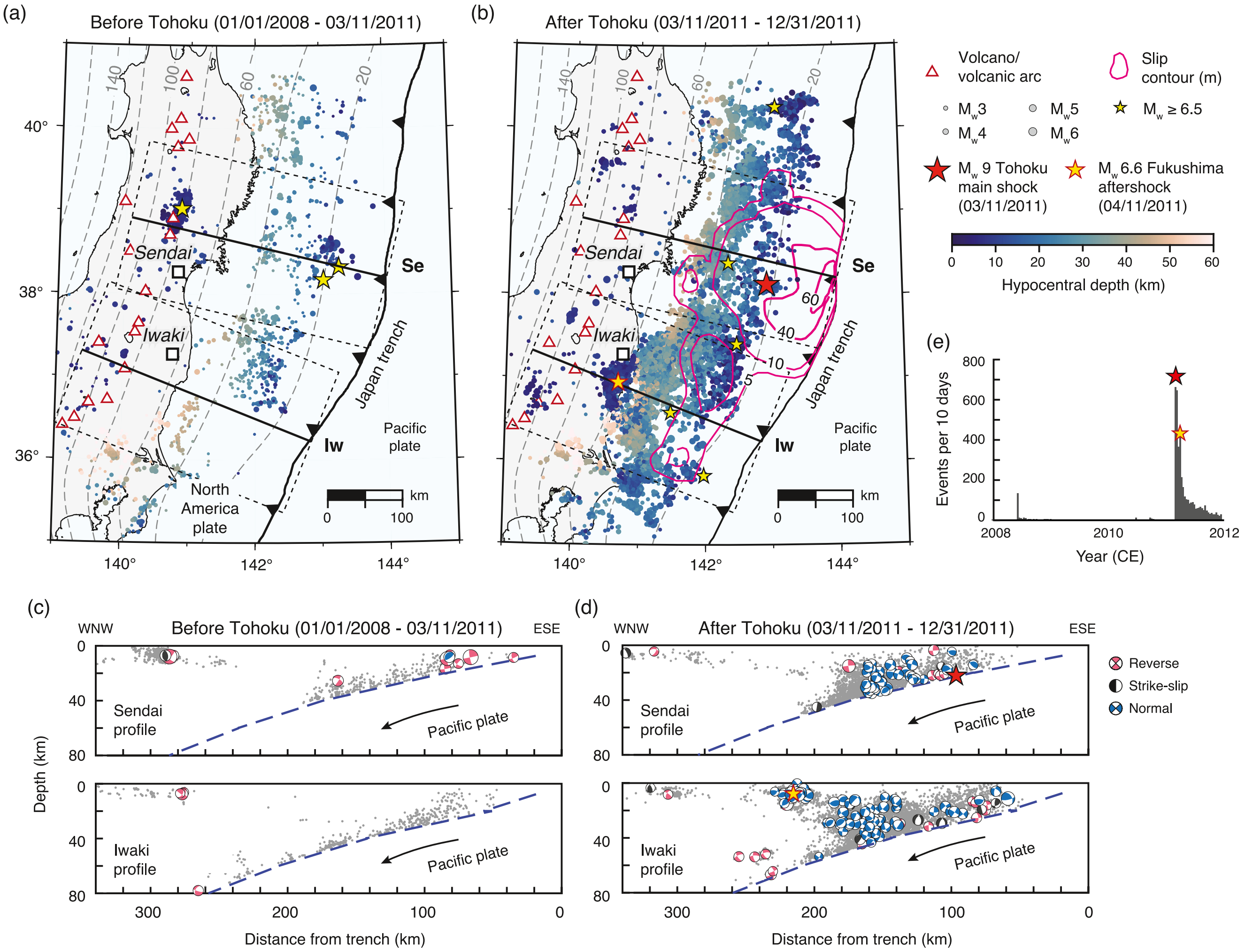

Figure 1. Seismotectonic setting of NE Japan. (a–d) Forearc seismicity before and after the Tohoku earthquake. (a, b) Map view. Black lines indicate location of cross-sections shown in (c) and (d). Dashed rectangles indicate the width of swaths (200 km) projected into the cross-sections. Se = Sendai, Iw = Iwaki. (c, d) Cross-sectional view. Gray dots are aftershock hypocenters from the Japan Meteorological Agency (JMA). Beach balls denote JMA focal mechanism solutions and are shown in profile view. Reverse faulting events in the outer marine forearc above the megathrust are likely poorly located interplate events (Nakamura et al., 2016) or the slab model is not accurate enough to classify them as interplate events. (e) Number of forearc earthquakes. Count includes events with magnitude ≥ magnitude of completeness ($M_c = 3.4$, Text S3 in Supporting Information S1).

an increase in fluid pressure (Terakawa et al., 2013) or the presence of small faults of variable orientation (Toda et al., 2011). CFS models commonly determine the stress change in the forearc solely from the earthquake slip distribution and neglect the total stresses in the forearc resulting from gravitational and megathrust shear stresses. The total stresses determine, however, the forearc stress state (i.e., the magnitude and orientation of principal stresses) and we show in Section 2 that the preseismic stress state affects the stress change in the forearc that results from a stress drop on the megathrust. Thus, assessing whether a megathrust stress drop supports or inhibits failure in the forearc requires detailed information on the preseismic or postseismic stress state.

For Japan, estimates of the megathrust stress drop and preseismic and postseismic stress states exist (Brodsky et al., 2020; Brown et al., 2015; Wang et al., 2019; Yang et al., 2013), but the available data do not allow an unambiguous assessment of forearc stress changes. We therefore pursue an innovative modeling approach that determines the preseismic and postseismic stress states and related stress change compatible with broad aftershock triggering due to the megathrust stress drop. Using the aftershock distribution and fault kinematics as modeling constraints allows determining the precise stress conditions required for triggering the bulk forearc seismicity that occurred in the first months after the Tohoku earthquake. The model results are supported by independent stress drop observations.

2. Modeling Approach

We use a plane-strain finite-element model of force balance following Wang et al. (2019) to assess the stress change caused by the megathrust stress drop. The model is created with the software ABAQUS and comprises a rigid lower plate in frictional contact with an elastic upper plate representing the forearc (Figure 2a, Text S1 and Figure S1 in Supporting Information S1). ABAQUS computes the total stress tensor in the upper plate resulting from all applied boundary conditions, including gravity, isostasy, and friction along the plate contact (megathrust). We compute gravitational stresses for average densities of 2,800 and 3,300 kg m^{-3} for crustal and mantle parts, respectively, and seawater load using a density of 1,025 kg m^{-3}. Gravitational acceleration is 9.81 m s^{-1}. Friction along the megathrust is generated by displacing the lower plate and computed for the effective friction coefficient μ' assigned to the megathrust, such that the megathrust shear stress τ is given by standard Coulomb friction ($\tau = \mu'\sigma_n$, where σ_n is normal stress).

To simulate the megathrust stress drop, the finite-element model includes a preseismic and a postseismic model step between which τ changes. The two model steps describe the stress state shortly before and after the megathrust earthquake, but not the stress state averaged over multiple earthquakes cycles as in other force-balance applications (Dielforder & Hampel, 2021; Lamb, 2006). Because τ also increases during earthquakes, e.g., due to fault strengthening processes downdip of the main rupture zone (Brown et al., 2015; Scholz, 1998), we divide the megathrust into fault weakening and fault strengthening segments (Figure 2a). The model implements weakening and strengthening behavior by decreasing and increasing the μ' values of fault segments between the preseismic and postseismic model steps, respectively. Because μ' is adjusted manually, the model does not involve a rate-and-state friction law and the results are independent of slip rate. As such, we do not model the coseismic stress evolution as in seismic cycle models (Sobolev & Muldashev, 2017; van Zelst et al., 2019).

To determine the forearc stress change as function of the preseismic and postseismic stress states, we solve the model for different pairs of preseismic and postseismic μ' values. We then determine the megathrust stress drop and resultant forearc stress change as difference in megathrust shear stress and forearc stress between the postseismic and preseismic model steps, respectively. Finally, we determine whether the stress change brings the forearc closer to or further from Coulomb failure in each model run. To do so, we first calculate the critical friction coefficient μ_c, for which faults in the forearc were critically stressed at the given stresses. Note that μ_c is calculated from the preseismic and postseismic model solutions using the Coulomb criterium for a cohesionless fault and is not a model input parameter (Text S2 in Supporting Information S1). If μ_c increases from the preseismic to the postseismic model step, the postseismic stresses support failure on stronger faults, which is compatible with an increase in seismicity after a megathrust earthquake. Conversely, If μ_c decreases, the stress change inhibits failure and seismicity and is incompatible with a seismicity increase. Accordingly, we can define the failure tendency $\Lambda = (\mu_{c,post} - \mu_{c,pre})/\mu_{c,pre}$ to describe whether the stress change supports ($\Lambda > 0$) or inhibits failure ($\Lambda < 0$).

Figure 2b illustrates the stress state in the forearc as function of μ' for an exemplary point in the outer forearc. The calculations were carried out for a generic forearc setup and varying μ' uniformly along the megathrust (Text S1 in Supporting Information S1). If μ' approaches zero, gravitational stresses dominate and the forearc experiences

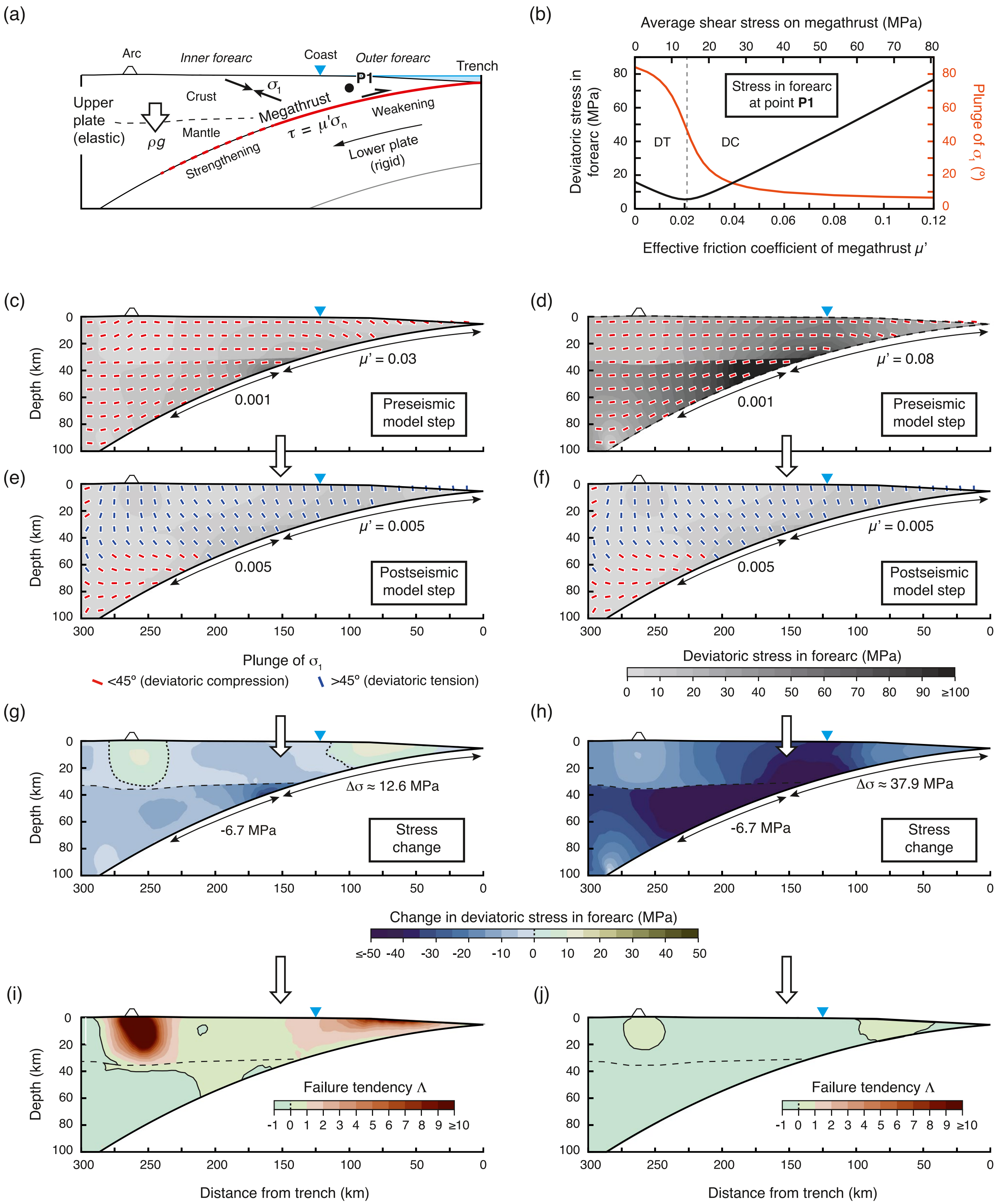

Figure 2. Model setup and generic models results. (a) Schematic representation of forearc model. Here, ρ is density, g is gravitational acceleration, μ' is the megathrust effective friction coefficient, τ and σ_n are the shear and normal stresses, respectively, and σ_1 is maximum compressive stress. (b) Deviatoric stress σ_{dev} (black) and plunge of σ_1 (orange) as function of μ' and average megathrust shear stress. Solutions are for site P1 in (a). DT and DC denote deviatoric tension and deviatoric compression, respectively. (c–j) Model results. (c–f) Deviatoric stress and plunge of σ_1 for preseismic and postseismic model steps. (g, h) Change in σ_{dev} due to megathrust stress drop $\Delta\sigma$. Positive and negative values of $\Delta\sigma$ indicate decrease and increase in megathrust shear stress, respectively. (i, j) Failure tendency Λ.

deviatoric tension (plunge of maximum compressive stress $\sigma_1 > 45°$). Conversely, as μ' increases, megathrust shear stresses dominate and the forearc experiences deviatoric compression (plunge of $\sigma_1 < 45°$). Note that for common μ' values of ≤ 0.06 (Gao & Wang, 2014) the deviatoric stress in the forearc and plunge of σ_1 do not vary linearly with μ' due to the opposing effect of gravitational and megathrust shear stresses on the stress field (Figure 2b). Thus, the stress change in the forearc and final stress state resulting from a change in τ depend on the initial megathrust shear stress (Figure S2 in Supporting Information S1). For example, a decrease in τ of 10 MPa from 35 to 25 MPa decreases the deviatoric stress by ~11 MPa while the stress state remains compressive. For comparison, a decrease in τ from 15 to 5 MPa increases the deviatoric by ~5 MPa but the stress state switches from deviatoric compression to tension (Figure 2b).

Figures 2c–2j illustrates for the generic forearc model that the failure tendency varies substantially with the preseismic stress state, even if the postseismic stress state is identical (note that μ' differs for the strengthening and weakening segments in these model runs). If the megathrust shear stress and forearc stress are low before the earthquake (Figure 2c), Λ increases in most of the forearc (Figure 2i). The increase in Λ results from two effects: first, the stress drop results in a reversal in the stress state from deviatoric compression to deviatoric tension, which supports failure because normal faulting operates at lower stresses than reverse faulting (Sibson, 1998). Second, the decrease in horizontal compression results in a net stress increase due to gravitational effects in areas of steep topography, such as the outer forearc (Figure 2g). For comparison, if the megathrust shear stress and forearc stresses are higher before the earthquake (Figure 2d), then the stress drop results in a net stress decrease, which tends to stabilize the forearc and causes low values of Λ, despite the concomitant stress reversal (Figure 2j). The stabilizing effect of the stress decrease reflects that the forearc must sustain much higher stresses before than after the earthquake, which makes postseismic failure unlikely. The effect of the stress decrease is also not counterbalanced by an increase in τ along the strengthening megathrust segment, which has a small impact on the stress in the inner forearc only. Consequently, only a narrow range of preseismic and postseismic stress states leads to an increase in Λ across the forearc.

3. Model Application to Japan and Discussion of Results

We apply our approach to Japan using finite-element models that account for margin topography, crustal thickness, water load, slab morphology, and extent of the seismogenic megathrust along the Sendai and Iwaki transects shown in Figure 1. We adjust the preseismic and postseismic μ' values of the weakening and strengthening megathrust segments until the following conditions are fulfilled: first, the bulk of aftershocks and seismic moment release occurs in areas of increased failure tendency. Second, the postseismic stress state is consistent with the prevailing fault kinematics in the forearc after the Tohoku earthquake (Figure 1d). These conditions are fulfilled for the preseismic and postseismic stress states shown in Figures 3a and 3b (Figure S3 in Supporting Information S1). The modeled stress change (Figure 3c) causes a failure tendency increase over large areas that encompass ~98% of the aftershocks and seismic moment release, while all normal faulting occurs in areas under deviatoric tension (Figures 3d and 3e). For comparison, slightly different preseismic and postseismic stress states are incompatible with the observed aftershock distribution and fault kinematics (Figures S4 and S5 in Supporting Information S1).

The modeled megathrust stress drop is spatially heterogeneous and differs for the Sendai and Iwaki transects (Figure 3c). The largest decrease in megathrust shear stress occurs at shallow and intermediate depth along the Sendai and Iwaki transects, respectively, resembling spatial differences in fault slip (Figure 1b). The stress drop along the weakening and strengthening fault segments varies between 18 and −12 MPa, respectively. The net stress drop averaged over the Sendai and Iwaki transects is ~2 MPa. The modeled stress drop is comparable to independent stress-drop estimates from 40 different slip-distribution models that vary between 30 and −20 MPa and yield a rupture-zone average <5 MPa (Brown et al., 2015; Wang et al., 2019). The megathrust stress drop in our models relates to changes in μ' along the weakening and strengthening segments of <0.02 (Figures 3a and 3b). The preseismic μ' values of the seismogenic megathrust vary between 0.02 and 0.025, in good agreement with previous estimates of ~0.02–0.03 derived from heat dissipation and force-balance models (Gao & Wang, 2014; Lamb, 2006; Seno, 2009; Wang et al., 2019).

The stress drop causes changes in deviatoric stress (σ_{dev}) from −10 to 20 MPa in the forearc (Figure 3c), while absolute values of σ_{dev} vary between 5 and 60 MPa both for the preseismic and postseismic model steps (Figures 3a and 3b). Megathrust stress drop, σ_{dev}, and change in σ_{dev} have the same order of magnitude, in agreement with

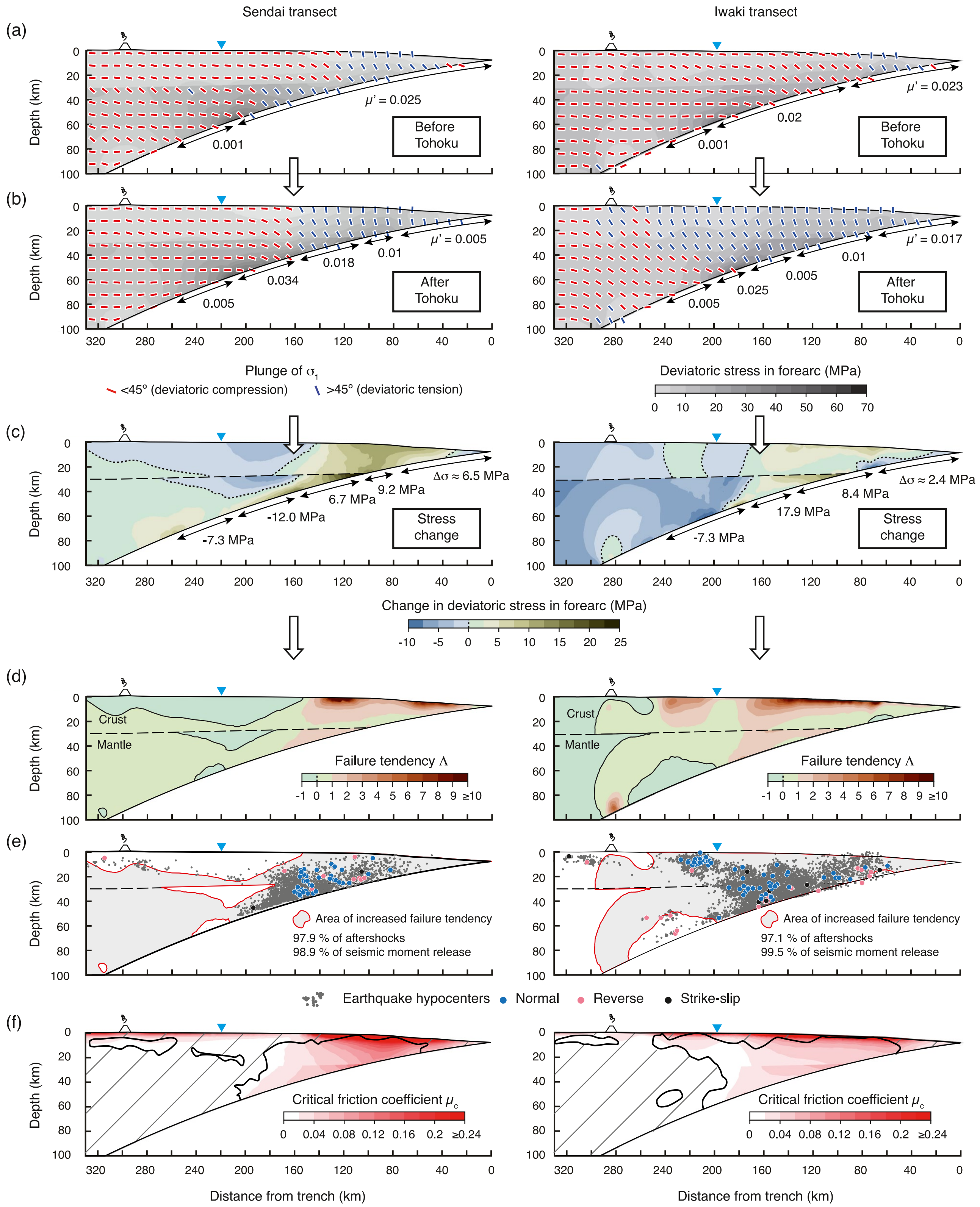

Figure 3. Model results for Japan. (a, b) Deviatoric stress and plunge of σ_1 for preseismic and postseismic model steps. (c) Change in σ_{dev} in the forearc due to megathrust stress drop $\Delta\sigma$. Positive and negative values of $\Delta\sigma$ indicate decrease and increase in megathrust shear stress, respectively. (d, e) Failure tendency Λ. Gray dots and red, blue, and black solid circles in (e) are hypocenters of forearc seismicity and reverse, normal, and strike-slip faulting events after the Tohoku earthquake, respectively (see Figure 1d). (f) Critical friction coefficient $\mu_{c,\mathrm{post}}$, which estimates the effective strength of faults in areas showing aftershock seismicity. Hatched areas indicate areas showing no seismicity, for which fault strength cannot be estimated.

previous estimates derived from stress reversals in the marine forearc (Hardebeck, 2012; Hasegawa et al., 2011). Furthermore, we find that the stress drop does not result in a general forearc stress decrease, but also in local stress increases. Interestingly, ∼78% of the aftershock seismicity and ∼92% of the seismic moment release occur in areas in which σ_{dev} increases (Tables S2 and S3 in Supporting Information S1). The areas lie within areas of increased failure tendency and encompass the marine forearc and coastal region near Iwaki (Figures 3b–3d). The megathrust stress drop and gravitational stresses arising from steep forearc topography control the σ_{dev} increase, particularly in the marine forearc. The topographic effect near Iwaki, however, is due to a local topographic high along the coast, the Abukuma plateau—a feature that is missing near Sendai (Figure S1b in Supporting Information S1). Our models, therefore, indicate that differences in forearc topography together with spatial stress drop differences have a discernible impact on forearc stress changes and likely facilitated the differences in coastal aftershock seismicity along strike of the forearc (Figure 1b). We also find a dearth of aftershock activity in forearc areas that experience a decrease in σ_{dev}, including inland Japan and the shelf region along the Sendai transect. Only the outermost marine forearc offshore Sendai deviates from this trend and shows little aftershock seismicity despite σ_{dev} increases.

Spatial variations in fault strength may govern spatial variability in aftershock seismicity (Wang et al., 2019). We therefore evaluate how the critical friction coefficient $\mu_{\mathrm{c,post}}$ varies across the forearc (Figure 3f). Parameter $\mu_{\mathrm{c,post}}$ is calculated from the postseismic stress solutions (Section 2) and is a composite parameter that includes the effects of both intrinsic friction and pore fluid pressure in the fault zone. It therefore provides an estimate for the effective strength of faults that were seismically active after the Tohoku earthquake. The effective fault strength in forearc areas showing no aftershock seismicity is likely higher than $\mu_{\mathrm{c,post}}$ as they seem not to have failed at the given stresses.

The $\mu_{\mathrm{c,post}}$ in the outermost forearc offshore Sendai is ∼0.075–0.24, i.e., highest in the forearc. The comparatively high strength may indicate that the outer forearc is generally stronger than more internal parts. Alternatively, the apparent strength may represent a postseismic condition and result from the large coseismic seaward displacement of the outer forearc, which exceeded 20 m above the main slip area close to the trench (Kido et al., 2011; Sato et al., 2011). The strong seaward displacement causes forearc dilation that tends to decrease pore pressures and increase fault strength (Manga et al., 2012). This interpretation is consistent with the higher seismicity in the outer forearc offshore Iwaki, where the seaward displacement was much smaller (∼5 m) and should not lead to a similar dilational strengthening effect.

Most aftershocks in both transects occur between ∼120 and ∼200 km from the trench and locate in the mantle wedge and overlying crust. The associated faults are likely very weak, in accordance with $\mu_{\mathrm{c,post}}$ values of ∼0.01–0.06 (Figure 3f). The low fault strength may relate to mantle wedge serpentinization and pressure buildup from fluids liberated from the subducting slab (Hyndman & Peacock, 2003; Tulley et al., 2022). Thus, the intense seismicity in the area may be linked to the position above the dehydrating slab.

Further inland, $\mu_{\mathrm{c,post}}$ is <0.02 for all but the upper 5–10 km of the forearc, and suggests that inland Japan hosts weak faults and quasi-lithostatic pore fluid pressures. In contrast to the mantle-wedge setting, high pore fluid pressures are likely locally restricted because of the large distance to the dehydrating slab. The local restriction of high fluid pressures is consistent with previous studies showing that the inland seismicity is linked to hydrothermal fluid migration along mature fault systems (Okada et al., 2011; Yoshida et al., 2017). The inland seismicity was also interpreted to have been triggered by local fluid pressure increases (Terakawa et al., 2013). A pressure increase would raise the failure tendency and may explain the seismicity underneath the volcanic arc not captured in our model (Figure 3e). Nevertheless, the low inland seismicity may be conditioned by very low background stresses that are marginally capable of initiating frictional failure, suggesting that these regions deform mainly viscously. Similar conditions will also apply to mantle areas that show very low or no seismic activity, although the failure tendency partially increases (Figures 3d and 3e).

4. Comparison of Model Stresses With Static Stress Drop of Forearc Earthquakes

Our models constrain the preseismic and postseismic stresses in the Japanese forearc. We now validate the stress solutions independently by comparison with static stress-drop estimates of earthquakes that occurred in the forearc before and after the Tohoku earthquake (Figure 4a). Earthquake stress drop magnitudes are restricted by the stress along the fault that ruptured and provide a lower bound for deviatoric stress derived from the

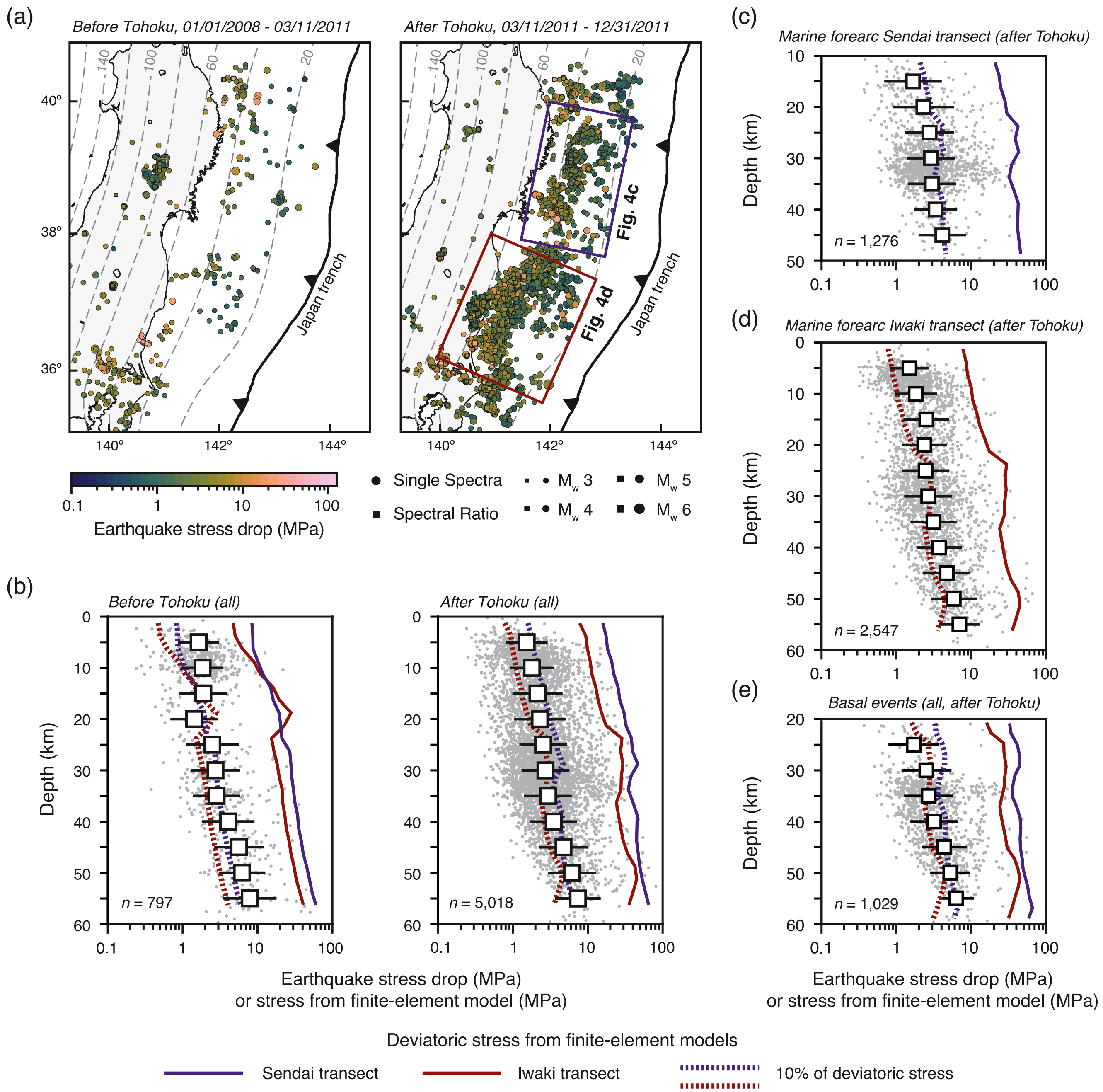

Figure 4. Earthquake stress drop values and comparison to model stresses (solid and dashed lines in c–e). (a, b) Earthquake hypocenters with estimated static stress drop. (c–e) Gray dots are individual stress-drop estimates (n = total number of estimates), squares are average stress drop values ($\overline{\Delta\sigma}_{\mathrm{Forearc}}$). Error bars represent one standard deviation. Basal events in (e) are events from 1 to 5 km above the slab interface.

finite-element models. In addition, spatiotemporal stress drop heterogeneities may hint at variations in ambient stresses (Kemna et al., 2021).

We estimate stress drop values using seismic data from the NIED High Sensitivity Seismograph Network (National Research Institute for Earth Science and Disaster Resilience, 2019) and the Japanese Meteorological Agency (JMA). As individual stress-drop estimates may reflect local stress heterogeneities that are not representative of average stresses, we first determine individual earthquake stress drop values using both single-spectra and spectral-ratio fitting methods. We then calculate average stress drop values ($\overline{\Delta\sigma}_{\mathrm{Forearc}}$) at 10-km depth intervals with 50% overlap (Text S3 and S4 and Figures S8 and S9 in Supporting Information S1). The averaged values better reflect bulk stress conditions in the forearc and are better suited for comparison with modeled stresses (Moyer et al., 2020).

The pre-Tohoku and post-Tohoku $\overline{\Delta\sigma}_{\text{Forearc}}$ values are largely similar and increase gradually with depth from ~2 to 8 MPa (Figure 4b). The stress drop estimation incorporates a depth-dependent velocity model from the JMA, thus the observed increase with depth is not an artifact of a constant shear velocity assumption (Abercrombie et al., 2021; Hauksson, 2015). A selection of similar event pairs within 5 km hypocentral distance further ensures a depth-dependent attenuation correction for stress drop values obtained using the spectral-ratio fitting method (Abercrombie et al., 2021; Figure S10 in Supporting Information S1). Aside from the depth dependency, the $\overline{\Delta\sigma}_{\text{Forearc}}$ values are spatially homogenous and do not vary significantly along forearc strike (Figure 4a). Likewise, stress drop values vary negligibly in time without a discernible trend (Figure S11d in Supporting Information S1). The range in estimated stress drop magnitudes presented here is consistent with previous estimates for the Japanese forearc (Yoshida et al., 2017).

We compare stress-drop estimates with model results by calculating the depth-dependent maximum values of σ_{dev} from the models for the Sendai and Iwaki transects (Figure 4b) and for the subregions that include most of the aftershocks (Figures 4c–4e). The depth-dependent deviatoric stresses are similar for the preseismic and postseismic states, which reflects that the maximum stresses did not change significantly due to the modeled stress drop. Similarity in the preseismic and postseismic σ_{dev} values resemble the constancy of $\overline{\Delta\sigma}_{\text{Forearc}}$ values. Moreover, the deviatoric stresses are generally higher than the stress-drop estimates, consistent with partial stress release during earthquakes (Brune, 1970; Simpson, 2018), and exhibit a similar depth dependency to $\overline{\Delta\sigma}_{\text{Forearc}}$. The remarkably consistent correlation across the forearc follows the trend of $\overline{\Delta\sigma}_{\text{Forearc}}$ being ~10% of σ_{dev} (Figures 4c–4e), suggesting that the average stress release scales with ambient stress. Taken together, we find that the deviatoric stresses obtained from the finite-element models agree favorably with the $\overline{\Delta\sigma}_{\text{Forearc}}$ values obtained from seismic data and validates the significance of the modeled forearc stresses.

5. Summary and Conclusions

We examine aftershock triggering by the stress drop of a megathrust earthquake and show that triggering is only possible for a narrow range of stress drop values and preseismic forearc stresses. We determine the range of values for the aftershock seismicity of the Tohoku earthquake using numerical force-balance models that are constrained by the observed aftershock distribution and fault kinematics. The model results are consistent with major aspects of the earthquake, including the magnitude and spatial heterogeneity of the stress drop, the strength of the Japanese megathrust, and the partial stress reversal in the forearc. Our models further indicate that ~78% of the aftershock seismicity and ~92% of the seismic moment release occurred in forearc areas of net stress increase, and that the detailed aftershock distribution was also governed by spatial variability in fault strength. Finally, we find that the modeled forearc stresses are remarkably consistent with independent estimates of earthquake stress drop values in the forearc before and after the Tohoku earthquake. Given the consistency in the data and its implications, we conclude that the bulk forearc seismicity in the first months after the Tohoku earthquake was triggered by the megathrust stress drop and resulting stress change in the forearc. This stress change will not remain unchanged after the megathrust earthquake but will be altered by viscoelastic relaxation processes, and relocking and reloading of the megathrust in the years after the megathrust earthquake (Bedford et al., 2016; Bürgmann et al., 2016; Sobolev & Muldashev, 2017; Sun et al., 2014). Viscoelastic relaxation and reloading tend to diminish the failure tendency and forearc seismicity with time. Whether the observed power-law like decrease in forearc seismicity already reflects these or other processes remains to be resolved. Independently, our approach helps to determine the stress perturbation in the forearc caused by the megathrust stress drop and can be applied to other great megathrust earthquakes to obtain detailed information on forearc stress and strength.

Data Availability Statement

Waveform data from the Hi-net borehole network of the National Research Institute for Earth Science and Disaster Resilience (2019). We downloaded Hi-net waveforms using the HinetPy package, Version 0.6.9 (https://10.5281/zenodo.4777177). Hypocentral locations and phase arrivals for Japan are available from the Japan Meteorological Agency (http://www.data.jma.go.jp/svd/eqev/data/bulletin/hypo.html). Estimated stress drop values, list of events used in this study, and ABAQUS output databases are available from https://doi.org/10.25835/0072357.

We used the mtspec Python wrapper for spectral estimations (Prieto et al., 2009). We process seismic data and create maps, swath profiles, and diagrams using the Python packages Obspy (Krischer et al., 2015), Matplotlib (Hunter, 2007), and GMT (Wessel et al., 2019). Color schemes follow *Scientific colour maps* (Crameri et al., 2020). The finite-element models were calculated, processed, and plotted using the commercial software packages ABAQUS and MATLAB and the Matlab tool Abaqus2Matlab by Papazafeiropoulos et al. (2017).

Acknowledgments

We thank S. Takemura (ERI, Japan) and D. Tian (MSU, USA) for the helpful suggestions on downloading and processing of Hi-net data from Japan. We thank the National Research Institute for Earth Science and Disaster Resilience and the Japan Meteorological Agency for granting open access to seismological data. Reviews by Iris van Zelst and an anonymous reviewer improved the clarity of the manuscript.

References

Abercrombie, R. E., Trugman, D. T., Shearer, P. M., Chen, X., Zhang, J., Pennington, C. N., et al. (2021). Does earthquake stress drop increase with depth in the crust? *Journal of Geophysical Research: Solid Earth*, *126*, e2021JB022314. https://doi.org/10.1029/2021JB022314

Bedford, J., Moreno, M., Li, S., Oncken, O., Baez, J. C., Bevis, M., et al. (2016). Separating rapid relocking, afterslip, and viscoelastic relaxation: An application of the postseismic straightening method to the Maule 2010 cGPS. *Journal of Geophysical Research: Solid Earth*, *121*, 7618–7638. https://doi.org/10.1002/2016JB013093

Brodsky, E. E., Mori, J. J., Anderson, L., Chester, F. M., Conin, M., Dunham, E. M., et al. (2020). The state of stress on the fault before, during, and after a major earthquake. *Annual Review of Earth and Planetary Sciences*, *48*(1), 49–74. https://doi.org/10.1146/annurev-earth-053018-060507

Brown, L., Wang, K., & Sun, T. (2015). Static stress drop in the M_w 9 Tohoku-oki earthquake: Heterogeneous distribution and low average value. *Geophysical Research Letters*, *42*, 10595–10600. https://doi.org/10.1002/2015GL066361

Brune, J. N. (1970). Tectonic stress and the spectra of seismic shear waves from earthquakes. *Journal of Geophysical Research*, *75*(26), 4997–5009. https://doi.org/10.1029/JB075i026p04997

Bürgmann, R., Uchida, N., Hu, Y., & Matsuzawa, T. (2016). Tohoku rupture reloaded? *Nature Geoscience*, *9*(3), 183. https://doi.org/10.1038/ngeo2649

Crameri, F., Shephard, G. E., & Heron, P. J. (2020). The misuse of colour in science communication. *Nature Communications*, *11*(1), 5444. https://doi.org/10.1038/s41467-020-19160-7

Cubas, N., Avouac, J.-P., Leroy, Y. M., & Pons, A. (2013). Low friction along the high slip patch of the 2011 M_w 9.0 Tohoku-Oki earthquake required from the wedge structure and extensional splay faults. *Geophysical Research Letters*, *40*, 4231–4237. https://doi.org/10.1002/grl.50682

Dewey, J. W., Choy, G., Presgrave, B., Sipkin, S., Tarr, A. C., Benz, H., et al. (2007). Seismicity associated with the Sumatra-Andaman Islands earthquake of 26 December 2004. *Bulletin of the Seismological Society of America*, *97*(1A), S25–S42. https://doi.org/10.1785/0120050626

Dielforder, A. (2017). Constraining the strength of megathrusts from fault geometries and application to the Alpine collision zone. *Earth and Planetary Science Letters*, *474*, 49–58. https://doi.org/10.1016/j.epsl.2017.06.021

Dielforder, A., & Hampel, A. (2021). Force-balance analysis of stress changes during the subduction-collision transition and implications for the rise of mountain belts. *Journal of Geophysical Research: Solid Earth*, *126*, e2020JB020914. https://doi.org/10.1029/2020JB020914

Di Toro, G., Han, R., Hirose, T., De Paola, N., Nielsen, S., Mizoguchi, K., et al. (2011). Fault lubrication during earthquakes. *Nature*, *471*(7339), 494–498. https://doi.org/10.1038/nature09838

Farías, M., Comte, D., Roecker, S., Carrizo, D., & Pardo, M. (2011). Crustal extensional faulting triggered by the 2010 Chilean earthquake: The Pichilemu Seismic Sequence. *Tectonics*, *30*, TC6010. https://doi.org/10.1029/2011TC002888

Gao, X., & Wang, K. (2014). Strength of stick-slip and creeping subduction megathrusts from heat flow observations. *Science*, *345*(6200), 1038–1041. https://doi.org/10.1126/science.1255487

Hardebeck, J. L. (2012). Coseismic and postseismic stress rotations due to great subduction zone earthquakes. *Geophysical Research Letters*, *39*, L21313. https://doi.org/10.1029/2012GL053438

Hasegawa, A., Yoshida, K., Asano, Y., Okada, T., Iinuma, T., & Ito, Y. (2012). Change in stress field after the 2011 great Tohoku-Oki earthquake. *Earth and Planetary Science Letters*, *355–356*, 231–243. https://doi.org/10.1016/j.epsl.2012.08.042

Hasegawa, A., Yoshida, K., & Okada, T. (2011). Nearly complete stress drop in the 2011 M_w 9.0 off the Pacific coast of Tohoku earthquake. *Earth Planets and Space*, *63*(7), 703–707. https://doi.org/10.5047/eps.2011.06.007

Hauksson, E. (2015). Average stress drops of Southern California earthquakes in the context of crustal geophysics: Implications for fault zone healing. *Pure and Applied Geophysics*, *172*(5), 1359–1370. https://doi.org/10.1007/s00024-014-0934-4

Hunter, J. D. (2007). Matplotlib: A 2D graphics environment. *Computing in Science & Engineering*, *9*(3), 90–95. https://doi.org/10.1109/mcse.2007.55

Hyndman, R. D., & Peacock, S. M. (2003). Serpentinization of the forearc mantle. *Earth and Planetary Science Letters*, *212*(3–4), 417–432. https://doi.org/10.1016/s0012-821x(03)00263-2

Kemna, K. B., Verdecchia, A., & Harrington, R. M. (2021). Spatio-temporal evolution of earthquake static stress drop values in the 2016–2017 central Italy seismic sequence. *Journal of Geophysical Research: Solid Earth*, *126*, e2021JB022566. https://doi.org/10.1029/2021JB022566

Kido, M., Osada, Y., Fujimoto, H., Hino, R., & Ito, Y. (2011). Trench-normal variation in observed seafloor displacements associated with the 2011 Tohoku-Oki earthquake. *Geophysical Research Letters*, *38*, L24303. https://doi.org/10.1029/2011GL050057

Krischer, L., Megies, T., Barsch, R., Beyreuther, M., Lecocq, T., Caudron, C., & Wassermann, J. (2015). ObsPy: A bridge for seismology into the scientific Python ecosystem. *Computational Science & Discovery*, *8*(1), 014003. https://doi.org/10.1088/1749-4699/8/1/014003

Lamb, S. (2006). Shear stresses on megathrusts: Implications for mountain building behind subduction zones. *Journal of Geophysical Research*, *111*, B07401. https://doi.org/10.1029/2005JB003916

Lange, D., Tilmann, F., Barrientos, S. E., Contreras-Reyes, E., Methe, P., Moreno, M., et al. (2012). Aftershock seismicity of the 27 February 2010 Mw 8.8 Maule earthquake rupture zone. *Earth and Planetary Science Letters*, *317–318*, 413–425. https://doi.org/10.1016/j.epsl.2011.11.034

Manga, M., Beresnev, I., Brodsky, E. E., Elkhoury, J. E., Elsworth, D., Ingebritsen, S. E., et al. (2012). Changes in permeability caused by transient stresses: Field observations, experiments, and mechanisms. *Reviews of Geophysics*, *50*, RG2004. https://doi.org/10.1029/2011RG000382

Moyer, P. A., Boettcher, M. S., Bohnenstiehl, D. R., & Abercrombie, R. E. (2020). Crustal strength variations inferred from earthquake stress drop at Axial Seamount surrounding the 2015 eruption. *Geophysical Research Letters*, *47*, e2020GL088447. https://doi.org/10.1029/2020GL088447

Nakamura, W., Uchida, N., & Matsuzawa, T. (2016). Spatial distribution of the faulting types of small earthquakes around the 2011 Tohoku-oki earthquake: A comprehensive search using template events. *Journal of Geophysical Research: Solid Earth*, *121*, 2591–2607. https://doi.org/10.1002/2015JB012584

National Research Institute for Earth Science and Disaster Resilience. (2019). *NIED Hi-net*. National Research Institute for Earth Science and Disaster Resilience. https://doi.org/10.17598/NIED.0003

Okada, T., Yoshida, K., Ueki, S., Nakajima, J., Uchida, N., Matsuzawa, T., et al. (2011). Shallow inland earthquakes in NE Japan possibly triggered by the 2011 off the Pacific coast of Tohoku earthquake. *Earth Planets and Space*, *63*(7), 749–754. https://doi.org/10.5047/eps.2011.06.027

Papazafeiropoulos, G., Muñiz-Calvente, M., & Martínez-Pañeda, E. (2017). Abaqus2Matlab: A suitable tool for finite element post-processing. *Advances in Engineering Software*, *105*, 9–16. https://doi.org/10.1016/j.advengsoft.2017.01.006

Parsons, T. (2002). Global Omori law decay of triggered earthquakes: Large aftershocks outside the classical aftershock zone. *Journal of Geophysical Research*, *107*(B9), 2199. https://doi.org/10.1029/2001JB000646

Prieto, G. A., Parker, R. L., & Vernon, F. L. (2009). A Fortran 90 library for multitaper spectrum analysis. *Computers & Geosciences*, *35*(8), 1701–1710. https://doi.org/10.1016/j.cageo.2008.06.007

Sato, M., Ishikawa, T., Ujihara, N., Yoshida, S., Fujita, M., Mochizuki, M., & Asada, A. (2011). Displacement above the hypocenter of the 2011 Tohoku-Oki earthquake. *Science*, *332*(6036), 1395. https://doi.org/10.1126/science.1207401

Scholz, C. H. (1998). Earthquakes and friction laws. *Nature*, *391*(6662), 37–42. https://doi.org/10.1038/34097

Seno, T. (2009). Determination of the pore fluid pressure ration at seismogenic megathrusts in subduction zones: Implications for strength of asperities and Andean-type mountain building. *Journal of Geophysical Research*, *114*, B05404. https://doi.org/10.1029/2008JB005889

Sibson, R. H. (1998). Brittle failure mode plots for compressional and extensional tectonic regimes. *Journal of Structural Geology*, *20*(5), 655–660. https://doi.org/10.1016/s0191-8141(98)00116-3

Simpson, G. (2018). What do earthquakes reveal about ambient shear stresses in the upper crust? *Geology*, *46*(8), 703–706. https://doi.org/10.1130/G45052.1

Sobolev, S. V., & Muldashev, I. A. (2017). Modeling seismic cycles of great megathrust earthquakes across the scales with focus at postseismic phase. *Geochemistry, Geophysics, Geosystems*, *18*, 4387–4408. https://doi.org/10.1002/2017GC007230

Sun, T., Wang, K., Iinuma, T., Hino, R., He, J., Fujimoto, H., et al. (2014). Prevalence of viscoelastic relaxation after the 2011 Tohoku-oki earthquake. *Nature*, *514*(7520), 84–87. https://doi.org/10.1038/nature13778

Terakawa, T., Hashimoto, C., & Matsu'ura, M. (2013). Changes in seismic activity following the 2011 Tohoku-oki earthquake: Effects of pore fluid pressure. *Earth and Planetary Science Letters*, *365*, 17–24. https://doi.org/10.1016/j.epsl.2013.01.017

Toda, S., & Stein, R. S. (2022). Central shutdown and surrounding activation of aftershocks from megathrust earthquake stress transfer. *Nature Geoscience*, *15*(6), 494–500. https://doi.org/10.1038/s41561-022-00954-x

Toda, S., Stein, R. S., & Lin, J. (2011). Widespread seismicity excitation throughout central Japan following the 2011 M=9.0 Tohoku earthquake and its interpretation by Coulomb stress transfer. *Geophysical Research Letters*, *38*, L00G03. https://doi.org/10.1029/2011GL047834

Tulley, C. J., Fagereng, Å., Ujiie, K., Diener, J. F. A., & Harris, C. (2022). Embrittlement within viscous shear zones across the base of the subduction thrust seismogenic zone. *Geochemistry, Geophysics, Geosystems*, *23*, e2021GC010208. https://doi.org/10.1029/2021GC010208

van Zelst, I., Wollherr, S., Gabriel, A.-A., Madden, E. H., & van Dinther, Y. (2019). Modeling megathrust earthquakes across scales: One-way coupling from geodynamics and seismic cycles to dynamic rupture. *Journal of Geophysical Research: Solid Earth*, *124*, 11414–11446. https://doi.org/10.1029/2019JB017539

Wang, K., Brown, L., Hu, Y., Yoshida, K., He, J., & Sun, T. (2019). Stable forearc stressed by a weak megathrust: Mechanical and geodynamic implications of stress changes caused by the M = 9 Tohoku-Oki earthquake. *Journal of Geophysical Research: Solid Earth*, *124*, 6179–6194. https://doi.org/10.1029/2018JB017043

Wang, K., & He, J. (1999). Mechanics of low stress forearcs: Nankai and Cascadia. *Journal of Geophysical Research*, *104*(B7), 15191–15205. https://doi.org/10.1029/1999JB900103

Wessel, P., Luis, J. F., Uieda, L., Scharroo, R., Wobbe, F., Smith, W. H. F., & Tian, D. (2019). The generic mapping tools version 6. *Geochemistry, Geophysics, Geosystems*, *20*, 5556–5564. https://doi.org/10.1029/2019GC008515

Yang, Y. R., Johnson, K. M., & Chuang, R. Y. (2013). Inversion for absolute deviatoric crustal stress using focal mechanisms and coseismic stress changes: The 2011 *M*9 Tohoku-oki, Japan, earthquake. *Journal of Geophysical Research: Solid Earth*, *118*, 5516–5529. https://doi.org/10.1002/jgrb.50389

Yoshida, K., Hasegawa, A., Okada, T., Iinuma, T., Ito, Y., & Asano, Y. (2012). Stress before and after the 2011 great Tohoku-oki earthquake and induced earthquakes in inland areas of eastern Japan. *Geophysical Research Letters*, *39*, L03302. https://doi.org/10.1029/2011GL049729

Yoshida, K., Hasegawa, A., Yoshida, T., & Matsuzawa, T. (2019). Heterogeneities in stress and strength in Tohoku and its relationship with earthquake sequences triggered by the 2011 M9 Tohoku-oki Earthquake. *Pure and Applied Geophysics*, *176*(3), 1335–1355. https://doi.org/10.1007/s00024-018-2073-9

Yoshida, K., Saito, T., Urata, Y., Asano, Y., & Hasegawa, A. (2017). Temporal changes in stress drop, frictional strength, and earthquake size distribution in the 2011 Yamagata-Fukushima, NE Japan, earthquake swarm, caused by fluid migration. *Journal of Geophysical Research: Solid Earth*, *122*, 10379–10397. https://doi.org/10.1002/2017JB014334

References From the Supporting Information

Abercrombie, R. E. (2021). Resolution and uncertainties in estimates of earthquake stress drop and energy release. *Philosophical Transactions of the Royal Society A: Mathematical, Physical & Engineering Sciences*, *379*(2196), 20200131. https://doi.org/10.1098/rsta.2020.0131

Amante, C., & Eakins, B. W. (2009). ETOPO1 1 Arc-Minute Global Relief model NOAA Technical Memorandum. https://doi.org/10.7289/V5C8276M

Bakun, W. H., & Bufe, C. G. (1975). Shear-wave attenuation along the San Andreas fault zone in central California. *Bulletin of the Seismological Society of America*, *65*(2), 439–459. https://doi.org/10.1785/bssa0650020439

Boatwright, J. (1980). A spectral theory for circular seismic sources; simple estimates of source dimension, dynamic stress drop, and radiated seismic energy. *Bulletin of the Seismological Society of America*, *70*(1), 1–27.

Cailleau, B., & Oncken, O. (2008). Past forearc deformation in Nicaragua and coupling at the megathrust interface: Evidence for subduction retreat? *Geochemistry, Geophysics, Geosystems*, *9*, Q03016. https://doi.org/10.1029/2007GC001754

Erdős, Z., Huismans, R. S., Faccenna, C., & Wolf, S. G. (2021). The role of subduction interface and upper plate strength on back-arc extension: Application to Mediterranean back-arc basins. *Tectonics*, *40*, e2021TC006795. https://doi.org/10.1029/2021TC006795

Eshelby, J. D. (1957). The determination of the elastic field of an ellipsoidal inclusion, and related problems. *Proceedings of the Royal Society of London Series A*, *241*, 376–396. https://doi.org/10.1098/rspa.1957.0133

Hampel, A., Lüke, J., Krause, T., & Hetzel, R. (2019). Finite-element modeling of glacial isostatic adjustment (GIA): Use of elastic foundations at material boundaries versus the geometrically non-linear formulation. *Computers & Geosciences*, *122*, 1–14. https://doi.org/10.1016/j.cageo.2018.08.002

Hanks, T. C., & Kanamori, H. (1979). A moment magnitude scale. *Journal of Geophysical Research*, *84*(B5), 2348–2350. https://doi.org/10.1029/JB084iB05p02348

Hayes, G. P., Moore, G. L., Portner, D. E., Hearne, M., Flamme, H., Furtney, M., & Smoczyk, G. M. (2018). Slab2, A comprehensive subduction zone geometry model. *Science*, *362*(6410), 58–61. https://doi.org/10.1126/science.aat4723

Ide, S., Beroza, G. C., Prejean, S. G., & Ellsworth, W. L. (2003). Apparent break in earthquake scaling due to path and site effects on deep borehole recordings. *Journal of Geophysical Research*, *108*(B5), 2271. https://doi.org/10.1029/2001JB001617

Iwasaki, T., Levin, V., Nikulin, A., & Iidaka, T. (2013). Constraints on the Moho in Japan and Kamchatka. *Tectonophysics*, *609*, 184–201. https://doi.org/10.1016/j.tecto.2012.11.023

Kanamori, H., & Anderson, D. L. (1975). Theoretical basis of some empirical relations in seismology. *Bulletin of the Seismological Society of America*, *65*(5), 1073–1095.

Kaneko, Y., & Shearer, P. M. (2015). Variability of seismic source spectra, estimated stress drop, and radiated energy, derived from cohesive-zone models of symmetrical and asymmetrical circular and elliptical ruptures. *Journal of Geophysical Research: Solid Earth*, *120*, 1053–1079. https://doi.org/10.1002/2014JB011642

Madariaga, R. (1976). Dynamics of an expanding circular fault. *Bulletin of the Seismological Society of America*, *66*(3), 639–666. https://doi.org/10.1785/bssa0660030639

Maeda, T., Obara, K., Furumura, T., & Saito, T. (2011). Interference of long-period seismic wavefield observed by the dense Hi-net array in Japan. *Journal of Geophysical Research*, *116*, B10303. https://doi.org/10.1029/2011JB008464

Newville, M., Stensitzki, T., Allen, D. B., Rawlik, M., Ingargiola, A., & Nelson, A. (2016). Lmfit: Non-linear least-square minimization and curve-fitting for Python. Astrophysics Source Code Library ascl: 1606.014.

Obara, K., Kasahara, K., Hori, S., & Okada, Y. (2005). A densely distributed high-sensitivity seismograph network in Japan: Hi-net by National Research Institute for Earth Science and Disaster Prevention. *Review of Scientific Instruments*, *76*(2), 021301. https://doi.org/10.1063/1.1854197

Pacor, F., Gallovic, F., Puglia, R., Luzi, L., & D'Amico, M. (2016). Diminishing high-frequency directivity due to a source effect: Empirical evidence from small earthquakes in the Abruzzo region, Italy. *Geophysical Research Letters*, *43*, 5000–5008. https://doi.org/10.1002/2016GL068546

Prieto, G. A., Parker, R. L., Vernon, F. L., Shearer, P. M., & Thomson, D. J. (2006). Uncertainties in earthquake source spectrum estimation using empirical green functions. In R. Abercrombie, A. McGarr, G. Di Toro, & H. Kanamori (Eds.), *Earthquakes: Radiated energy and the physics of faulting*. https://doi.org/10.1029/170GM08

Schwanghart, W., & Scherler, D. (2014). TopoToolbox 2—MATLAB-based software for topographic analysis and modeling in Earth surface sciences. *Earth Surface Dynamics*, *2*, 1–7. https://doi.org/10.5194/esurf-2-1-2014

Thomson, D. J. (1982). Spectrum estimation and harmonic analysis. *Proceedings of the IEEE*, *70*(9), 1055–1096. https://doi.org/10.1109/proc.1982.12433

Wada, I., & Wang, K. (2009). Common depth of slab-mantle decoupling: Reconciling diversity and uniformity of subduction zones. *Geochemistry, Geophysics, Geosystems*, *10*, Q10009. https://doi.org/10.1029/2009GC002570

Erratum

Due to a typographical error introduced in the originally published version of this article, the National Research Institute for Earth Science and Disaster Resilience and the Japan Meteorological Agency were credited with funding this research. The study was conducted without funding. This error has since been corrected, and the present version may be considered the authoritative version of record.